

THE SURFACE ALBEDO OF THE VATNAJÖKULL ICE CAP, ICELAND: A COMPARISON BETWEEN SATELLITE-DERIVED AND GROUND-BASED MEASUREMENTS

CARLEEN H. REIJMER, WOUTER H. KNAP * and JOHANNES OERLEMANS
Institute for Marine and Atmospheric Research Utrecht, University of Utrecht, Princetonplein 5, 3584 CC Utrecht, The Netherlands

(Received in final form 20 November 1998)

Abstract.

The temporal and spatial variations in the surface albedo of the Vatnajökull ice cap, Iceland, are investigated. A time series of the surface albedo is composed for the summer of 1996 using satellite radiance measurements from the Advanced Very High Resolution Radiometer (AVHRR). This time series is compared with ground measurements carried out during a glacio-meteorological experiment during the same summer on the ice cap. The AVHRR is able to reproduce the development in time of the surface albedo fairly well. The large systematic differences found for some of the stations on the ice are attributed to sub-pixel scale variations in the albedo. An attempt is made to confirm this hypothesis using satellite radiance measurements carried out by the Thematic Mapper (TM) and measurements made with a portable albedometer. The TM has a pixel size of 30×30 m whereas the pixel size of the AVHRR is 1×1 km. Although the TM measurements show greater variability in the albedo than do the AVHRR measurements, the large systematic difference remains. Measurements with the portable albedometer show a large spread in the albedo at sites with large systematic differences. This implies that the scale of the albedo variations is smaller than the scale of the AVHRR and TM pixels.

Keywords: Surface albedo, Iceland, Satellite-derived measurements, Temporal variability, Spatial variability

1. Introduction

The melting of glaciers and small ice caps on time scales of decades to a century is believed to contribute significantly to sea level rise ($\approx 20\%$) (Houghton *et al.*(1995)). Therefore, knowledge of the mass balance of glaciers and small ice caps is of great importance. In sub-polar and temperate climates, the mass balance is usually to a large extent determined by the summer energy balance (see e.g. Ambach(1963) for the central-western part of the Greenland ice sheet). Solar radiation provides by far the most energy for melting. Since the surface albedo controls the amount of absorbed solar radiation, this quantity is a key parameter in models designed for the calculation of glacier melt. The parameterization of the albedo in models is often based on field measurements carried out with a limited

* Present affiliation: Royal Netherlands Meteorological Institute P.O. Box 201, 3730 AE De Bilt, The Netherlands



number of instruments on a glacier. Due to the variability of the ice albedo these few point measurements may not be representative for the entire glacier; satellite data have the potential to overcome this problem. Nevertheless, ground measurements are still necessary to improve retrieval methods and to verify the satellite-derived albedos. Studies to improve parts of the retrieval method have been carried out by e.g. Li and Leighton(1992) , Knap and Reijmer(1998) and Knap *et al.*(1999). Attempts to compare ground-based and satellite-derived albedos have been made infrequently (Hall *et al.*(1990); Koelemeijer *et al.*(1993); Knap and Oerlemans(1996); Knap *et al.*(1998))

In this paper the temporal and spatial variations in the surface albedo of the Vatnajökull ice cap, Iceland, are described using ground measurements and NOAA AVHRR (Advanced Very High Resolution Radiometer) satellite data. Knap and Oerlemans(1996) carried out a similar study in the Søndre Strømfjord area, western Greenland. They suggested that the difference between ground measurements and satellite measurements were caused mainly by the different fields of view of the instruments used (1×1 km for AVHRR and 10×10 m for ground measurements) together with the scale of variations in the physical composition of the surface. Therefore, in this paper AVHRR sub-pixel variation in the surface albedo is studied on the basis of high resolution Landsat-5 TM (Thematic Mapper) satellite data and ground-based measurements.

The in-situ data used were gathered during a glacio-meteorological experiment on the ice cap in the summer of 1996 (TEMBA(1997)) (Figure 1). The general goal of the experiment was to extend our knowledge of the relation between glacier behaviour and climate change. More specific goals were to obtain a good estimate of the mass balance of the ice cap, its spatial variability and its sensitivity to climate change. Furthermore, our aim was to measure the surface energy balance of the entire ice cap during the summer of 1996 and to use the data set for validating surface parameters determined from satellite observations.

The ice cap is situated in a maritime climate with low summer temperatures (maximum average temperature of 11°C in the warmest months) and high winter precipitation (maximum annual precipitation more than 4000 mm). The Vatnajökull ice cap is the largest (≈ 8300 km²) ice cap of Europe situated in the south eastern part of Iceland. The altitude extends from 100 m to 2120 m a.s.l.. All the glaciers of the ice cap are of the temperate type.

2. Instruments and data

2.1. GROUND-BASED INSTRUMENTS

The universities of Amsterdam (The Netherlands), Innsbruck (Austria), Reykjavik (Iceland) and Utrecht (The Netherlands) participated in the glacio-meteorological experiment in the summer of 1996 and performed detailed meteorological measurements. A total of 16 meteorological stations on and near the ice cap were established

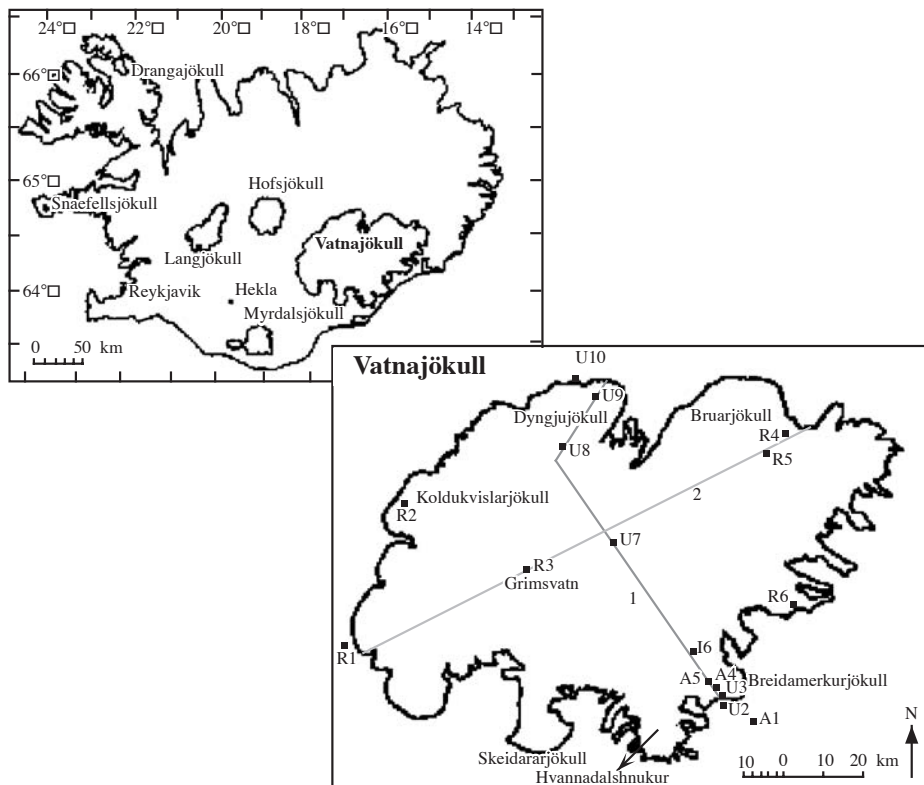


Figure 1. Geographical setting of the Vatnajökull ice cap, Iceland. The numbered dots indicate the locations of the 16 meteorological stations during the experiment in the summer of 1996. A = Amsterdam free university, I = Innsbruck university, R = Reykjavik university and U = Utrecht university. The lines 1 and 2 represent transect 1 and transect 2, respectively.

along two transects (Figure 1). At nine of the stations on the ice cap (A4, A5, I6, U7, U8, U9, R2, R4, and R5) albedo measurements were carried out automatically by measuring the incoming and outgoing short-wave radiation fluxes using Kipp & Zonen pyranometers (type CM7, CM14 and CM21). The instruments used were all sensitive to wavelengths of 0.30 - 2.8 μm and were placed in a horizontal position, with the measuring heights varying between 1 and 3 m. The surface area covered by the instruments depended on the height of the instruments and varied roughly between $4 \times 4 \text{ m}^2$ and $10 \times 10 \text{ m}^2$.

We carried out additional measurements with a portable albedometer (Van der Hage(1992)) near sites A4, A5, U7 and U8 to obtain a better idea of the spatial distribution of the albedo surrounding these sites. These measurements were done on a 25-point grid of $40 \times 40 \text{ m}$ around the pyranometer (Figure 2).

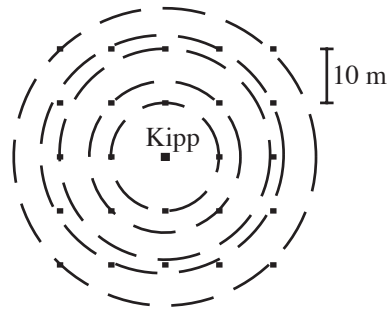


Figure 2. The grid (black squares) around the pyranometer measured with the portable albedo meter.

Table I. AVHRR and TM spectral bands

	Channel	Wavelength (μm)	
AVHRR	1	0.58-0.68	visible
	2	0.72-1.10	near-infrared
TM	2	0.52-0.60	visible
	4	0.76-0.90	near-infrared

2.2. SATELLITE INSTRUMENTS

In the present study data from instruments carried by the NOAA-14 satellite and the Landsat-5 satellite are used. Both satellites are polar orbiting and employ a multi-spectral scanners which measure reflected solar radiation in distinct intervals of the electromagnetic spectrum. The repeat time of the NOAA-14 is 1 day, whilst the repeat time of the Landsat-5 is 16 days (Lillesand and Kiefer(1987)). The multi-spectral scanner carried by the NOAA-14 satellite is the Advanced Very High Resolution Radiometer (AVHRR), and measures radiation reflected and emitted by the earth's surface in 5 spectral intervals. Channels 1 and 2 are used to derive the surface albedo (Tab. I). The resolution of the AVHRR ranges from 1.1×1.1 km at nadir to 2.2 km (along track) by 6.9 km (across track) at maximum off-nadir ($\pm 55.4^\circ$ off-nadir). The Landsat-5 employs the Thematic Mapper (TM), a multi-spectral scanner, which measures radiation in 7 distinct intervals; we use channels 2 and 4 of this instrument (Tab. I). The spatial resolution of the TM is 30×30 m except for channel 6, which has a resolution of 120×120 m. The resolution of the TM remains approximately the same at nadir and at maximum off-nadir, due to the small sweep angle, of 14.92° .

In Iceland, cloud cover regularly hampers the acquisition of usable images. Therefore, the AVHRR data were used to produce a time series of the surface albedo of the

ice cap during the summer of 1996 because the AVHRR has a better repeat time. The TM data are used to study the variability of the surface albedo on a scale of 30 m. Both AVHRR and TM data are compared with the ground measurements.

3. Retrieval method

In this section a brief description is given of how we derived the surface albedo from the AVHRR and TM satellite data.

3.1. PLANETARY ALBEDO

First we calculated the planetary bidirectional reflectance for AVHRR ($r_{pla,AVHRR}$) and TM ($r_{pla,TM}$) on the basis of the following relationships (note that we have omitted subscripts relating to the different wavelength bands):

$$r_{pla,AVHRR} = \frac{d^2(SC + I)}{\cos \theta_s}, \quad (1)$$

$$r_{pla,TM} = \frac{\pi d^2 c(t)(A_0 + A_1 Q_{cal})}{E_{sun} \cos \theta_s}. \quad (2)$$

The recorded count levels for AVHRR and TM are given by C and Q_{cal} , respectively; calibration coefficients are S and I for AVHRR and A_0 and A_1 for TM. In both expressions d is the Sun-Earth distance. The denominator of 3 represents the band solar irradiance at the top of the earths atmosphere (E_{sun} is the band solar constant and θ_s is the solar zenith angle). For AVHRR the solar constant is included in the calibration procedure, so this term does not occur in 2. Degradation of TM (i.e., time-dependent reduction of the responsivity of the instrument) is governed by the parameter $c(t)$ in 3, which was calculated on the basis of data presented by Thome *et al.*(1993) and Thome (personal communication). Further details of the procedure are discussed by Knap *et al.*(1998). Degradation of AVHRR is taken into account in the calibration factors S and I . Values of all parameters occurring in 2 and 3 are listed in II.

Since no detailed information is available about the anisotropy of the surface-atmosphere system, it was assumed that the reflected radiation field at the top of the earths atmosphere is isotropic. This implies that there is no difference between reflectance (r) and albedo (i.e., hemispherically averaged reflectance) (α) so we may write $\alpha_{pla,AVHRR} = r_{pla,AVHRR}$, and, similarly, $\alpha_{pla,TM} = r_{pla,TM}$. According to Knap and Reijmer(1998) this assumption may introduce significant errors in the satellite-derived albedos. Their results show an underestimation of the ice albedo of 0.05 independent of the magnitude of the albedo. These numbers were derived for

Table II. Post-launch calibration coefficients S and I revised on 31 July 1995 for NOAA-14 AVHRR. (Amendments to NOAA technical memorandum 107; Appendix-B). Calibration coefficients A_0 and A_1 for Landsat-5 TM representative for 1000 days after launch (Epema(1990)). E_{sun} is the mean solar irradiance at the top of the atmosphere in the TM band and $c(t)$ is the correction factor for images acquired more than 1000 days after launch.

	AVHRR 1	AVHRR 2
S	0.1115	0.1337
I	-4.5715	-5.4817
	TM 2	TM 4
A_0	-0.15732	-0.23286
A_1	0.11958	0.12564
E_{sun}	150.0	134.0
c (Aug. '95)	1.1014 ± 0.05	1
c (Aug. '96)	1.1137 ± 0.05	1

solar zenith angles between 46° and 49° and for nadir view angles. The magnitude of the error depends on the solar zenith angle and the view angles. The underestimation of the snow albedo is smaller, less than 5% of the snow albedo under the same conditions (Suttles *et al.*(1988)). Therefore, the impact of this assumption will be larger for ice albedos than for snow albedos. The results of Knap and Reijmer(1998) are based on ground-based measurements. The results of Suttles *et al.*(1988) are based on satellite-derived measurements from the Earth Radiation Budget Experiment.

3.2. SURFACE ALBEDO

To obtain a surface albedo (α_{sfc}) the planetary albedo (α_{pla}) has to be corrected for the presence of the atmosphere. The following relationship is used to correct for the presence of the atmosphere (the subscripts indicating the instrument have been omitted):

$$\alpha_{sfc} = a + b\alpha_{pla} + c\alpha_{pla}^2 . \quad (3)$$

The coefficients a , b and c depend on the thermodynamic structure of the atmosphere, the atmospheric constituents, the solar elevation, the height of the surface and the part of the electromagnetic spectrum used. The coefficients a , b and c are determined by

using a two-stream radiative transfer model based on Slingo and Schrecker(1982) . The model calculates α_{pla} for a given α_{sfc} on a range of α_{sfc} . As input, the model uses the sub-Arctic summer profiles (SASP) presented by McClatchey *et al.*(1972), the elevation of the surface and the solar zenith angle. Aerosols are not included. Relationship 3 is a near-perfect fit of the model results with a root mean square (rms) value of the residuals of $\sigma_{res} = 0.001$. The atmosphere correction introduces only minor uncertainties (< 0.01), with the main errors arising out of the use of SASP and omission of aerosols. Fortunately, the model is not very sensitive to realistic changes in profiles and the role of aerosols is probably limited because the ice cap is situated far away from sources of substantial aerosol emissions. Furthermore, the model reproduces the transmissivity of the atmosphere properly (Reijmer(1997)).

3.3. SPECTRALLY INTEGRATED ALBEDO

Using 2, 3 and 3 we were able to calculate the narrowband planetary and surface albedos for the visible and near-infrared wavelength bands of TM and AVHRR. However, for energy balance applications one is interested primarily in the spectrally integrated (i.e. broad-band) albedo. The conversion from narrow-band to broad-band albedo was carried out on the basis of empirical relationships established by Li and Leighton(1992) for AVHRR and Knap *et al.*(1999) for TM. The expressions for the broad-band albedos (α_{AVHRR} and α_{TM}) read:

$$\alpha_{AVHRR} = 4.53 + 0.389\alpha_{AVHRR1} + 0.452\alpha_{AVHRR2} \quad (4)$$

and

$$\alpha_{TM} = 0.726\alpha_{TM2} - 0.322\alpha_{TM2}^2 - 0.051\alpha_{TM4} + 0.581\alpha_{TM4}^2, \quad (5)$$

where the additional subscripts refer to AVHRR bands 1 and 2 and TM bands 2 and 4. Note that Li and Leighton(1992) established their conversion relationship on the basis of satellite data (AVHRR and ERB measurements made over polar regions north of 60°N), whereas Knap *et al.*(1999) used ground-based measurements (made on the Morteratsch glacier, Switzerland). This implies that the narrow-band albedos in 4 and 5 refer to planetary and surface albedos, respectively. Consequently, 4 should be applied *before* the atmospheric correction and 5 *after* it. The errors introduced by the spectral integration is small. Li and Leighton(1992) present a rms error of 2% in their narrowband to broadband conversion (4) and Knap *et al.*(1999) present a rms difference of 0.009 between modelled and measured albedo (5).

3.4. GEOLOCATION

In order to intercompare different satellite images and to compare satellite-derived surface albedos with ground-based measurements the images need to be geolocated as accurately as possible. The AVHRR images were geolocated and transformed into a cylindrical stereographic projection by the NERC satellite Station (University of Dundee, UK). Furthermore, the AVHRR pixels were resampled to equal sizes of approximately 1×1 km to prevent loss of resolution. These corrections provide images with an absolute location accuracy of about 15 km. The TM images were System Corrected and delivered by Eurimage (Frascati, Italy) and had an absolute location accuracy of about 500 m. The accuracy of both kinds of images is clearly not good enough. To couple pixel co-ordinates to geographical co-ordinates the following linear transformation was used:

$$\begin{pmatrix} l_1 \\ l_2 \end{pmatrix} = \begin{pmatrix} d_{11} & d_{12} \\ d_{21} & d_{22} \end{pmatrix} \begin{pmatrix} k_1 \\ k_2 \end{pmatrix} + \begin{pmatrix} e_1 \\ e_2 \end{pmatrix}. \quad (6)$$

In this relation (l_x, l_y) are the image co-ordinates (representing pixels of 30 m or 1 km squared) relating to (k_x, k_y) , the geographical co-ordinates obtained from general section maps of Iceland (Iceland Geodetic Survey, leaf 8 & 9, 1 : 250000). The coefficients d_{ij} and e_i are different for each scene, and were determined with linear regressions using 3 ground control points. It is estimated that the ground measurements can now be found within an area of 3×3 pixels.

4. Results

In this section the results will be described. We used four types of instruments to determine the surface albedo: the satellite instruments TM and AVHRR, the automatically measuring ground-based pyranometers and the portable albedometer. In Section 4.1 we describe the evolution of the in-situ albedo by means of the ground-based measurements using the pyranometers, to provide insight into the temporal and spatial variability of the surface albedo of the Vatnajökull. In Section 4.2 the AVHRR images are described; these provide insight into the temporal and spatial variability of the surface albedo of the Vatnajökull on a larger scale. The AVHRR images are used in Section 4.3 in the inter-comparison between AVHRR-derived and ground-based measured surface albedo. In Section 4.4 we try to explain the differences found between AVHRR-derived and ground-based measured surface albedo by comparing TM-derived surface albedo with in-situ measurements (automatic and portable albedo measurements). We conclude the description of the results in Section 4.5 with a comparison between AVHRR-derived and TM-derived surface albedos.

4.1. EVOLUTION OF THE IN-SITU ALBEDO

The albedos presented here are daily means calculated from hourly (Reykjavik and Innsbruck sites), 30 minute (Amsterdam sites) and 2 minute means (Utrecht sites) ground-based measurements of incoming and outgoing short-wave radiation.

Figure 3 shows the time-dependent evolution of the surface albedo during the 1996 field experiment, with Figure 3a showing the surface albedos for sites A4, A5 and I6. These sites were situated on the Breidamerkurjökull, a large outlet glacier in the southern part of the ice cap. The figure shows a decrease in the surface albedo during the melt season, the high albedo values at the beginning of the measuring period (May) indicating that the surface was snow-covered. The arrows in the figure indicate snowfall events deduced from the peak values in the albedo. After the snow has melted, and bare ice was exposed (June), a strong reduction in the albedo occurs in the course of the melt season. The largest decrease from 0.55 in June to 0.1 in August occurred near I6. The small variations in albedo are probably produced by different cloud cover conditions and variations in the amount of melt water. After the snow had melted, large patterns of channels draining melt water emerged; these channels were 0.5 to 2 m deep, a few metres wide and ran more or less parallel to the slope of the glacier. Between the channels were plateaus of clean ice that were a few metres wide and long. The patterns were most pronounced near I6 and less pronounced closer to the ice margin. In the channels dust and moraine material accumulated causing the strong reduction in the albedo in the course of the melt season.

Figure 3b shows the surface albedo of the three highest sites (U7, U8, and R5) on the ice cap, with site U7 placed in the accumulation area of the ice cap. The surface near site U7 consisted of snow for the entire season and therefore the albedo remained high (between 0.7 and 0.9). At the beginning of the field campaign the snow was probably dry, and until 10 June the temperature stayed below 0°C throughout day. Subsequently, melting of the snow cover caused the albedo to drop from 0.85 to 0.70; occasional large increases in albedo are most probably the result of fresh snow. Snowfall events are indicated with arrows and deduced from peaks in the albedo and measurements with an acoustic snow-height altimeter. Sites R5 and U8, situated on the higher parts of the Bruarjökull and the Dyngjujökull respectively, show almost the same pattern as that seen at site U7. The lower albedo near R5 compared to U7 is probably caused by a larger amount of melt water percolating the snow; near U8 the snow melted away entirely exposing very dirty glacier ice (surface albedo <0.1).

Sites R2, R4 and U9 were situated on glaciers in the northern region of the ice cap; R2 was near the margin of the Koldukvislarjökull, U9 on the Dyngjujökull and R4 on the Bruarjökull. Figure 3c shows the albedo development for these sites. At these stations the snow cover melts away entirely and glacier ice covered with black volcanic dust is exposed. The abundance of black volcanic dust causes the albedo to become extremely low, less than 0.1 near sites U9 and R2 and approximately 0.2

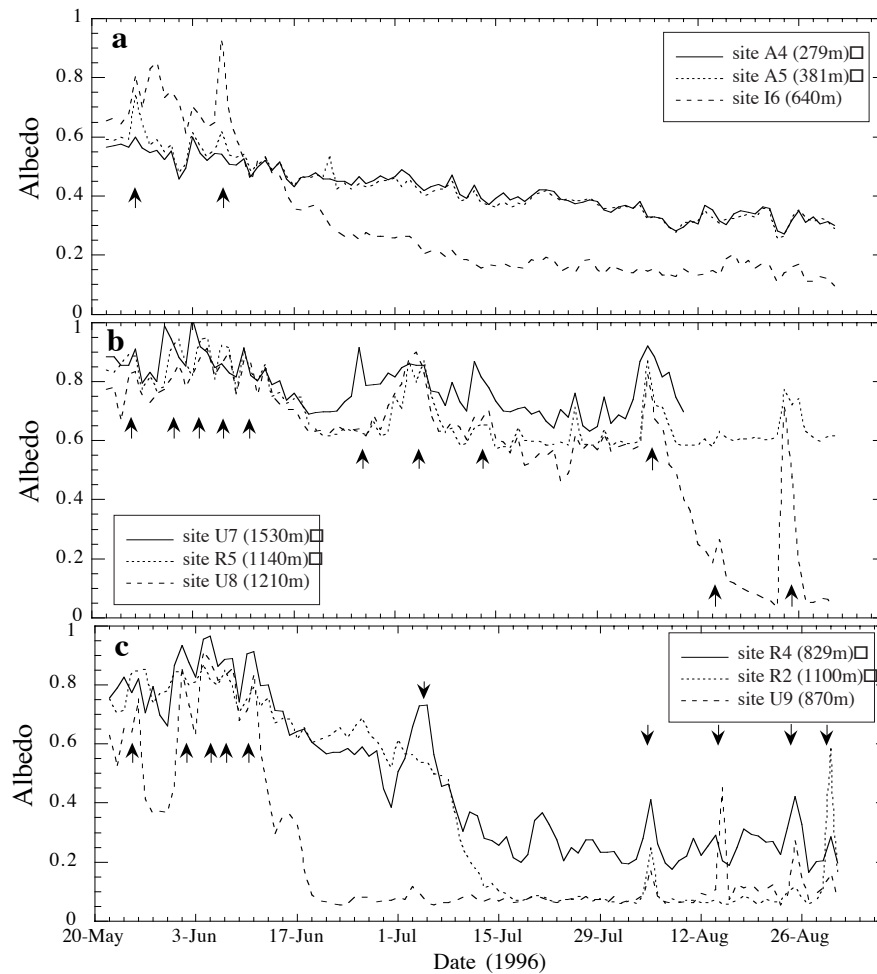


Figure 3. In-situ measured daily mean surface albedo. Arrows indicate snow-fall events. Sites A4, A5 and I6 are presented in (a), sites U7, U8, and R5 are presented in (b) and sites R2, R4, and U9 are presented in (c). The elevation above sea level of the sites is given as well.

near site R4. As the sites R2 and U9 lie in a volcanically active area, the albedo is lower than at R4 outside this area (Björnson(1990)).

4.2. THE SATELLITE-DERIVED SURFACE ALBEDO, A TIME SERIES

To compose a time series of the albedo, we used 11 AVHRR images that covered a large part of the ablation season. The images give an impression of the two-dimensional distribution and the development of the albedo over time; Figure 4 shows a selection of four of the images. Marked areas are regions with possible cloud cover identified from the visible and near-infrared channels as well as the mid-infrared and thermal-infrared channels of the satellite instrument; these regions

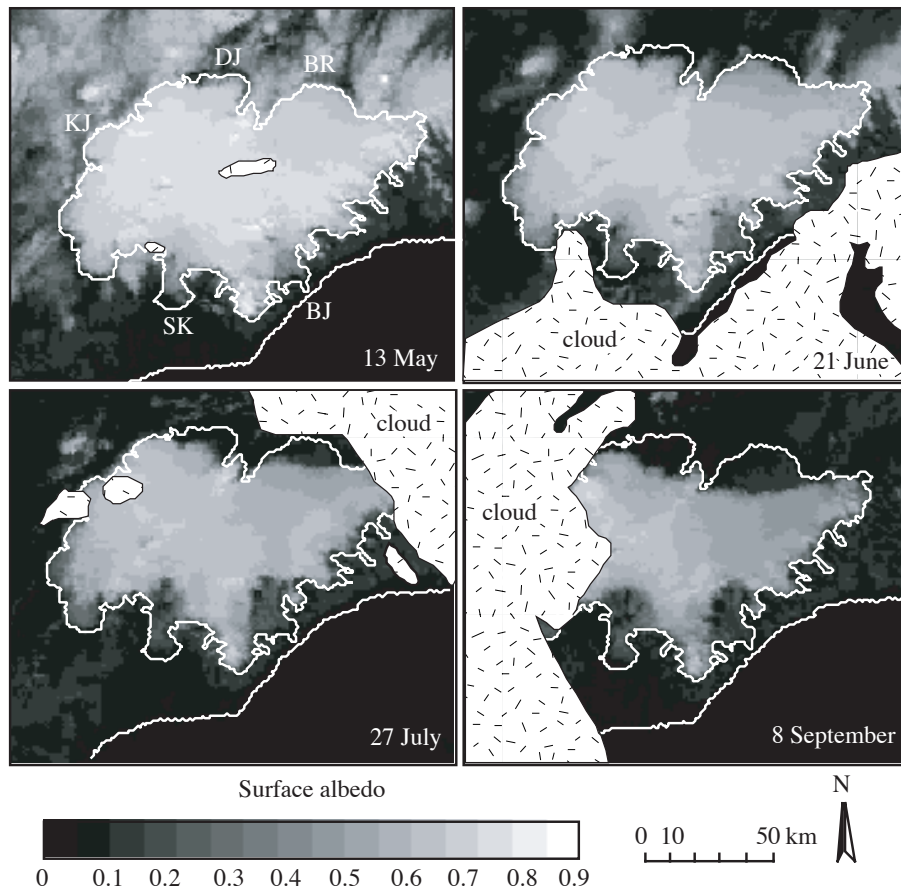


Figure 4. Satellite-derived surface albedo of the Vatnajökull ice cap. A selection of 4 out of a total of 11 images is made. Marked areas are regions with possible cloud cover. BJ = Breidamerkurjökull, SK = Skeidarárjökull, KJ = Koldukvislarjökull, DJ = Dyngjujökull, BR = Brúarjökull.

are marked by hand. The images show that at higher elevations the surface remains covered with snow, and the albedo decreases from 0.80 to 0.60 during the melt season. This reduction is likely to be caused by wetting of the snowpack, which is in agreement with Williams(1987) who suggested the absence of dry snow on the ice cap in the melt season. After the snow has melted at the surface of the outlet glaciers, the ice proves to be highly spatially variable, especially in the southern outlet glaciers. The ice albedo of the northern outlets is generally lower than that of the southern outlets (0.1 compared to 0.2) and shows little variation. In the south the ice albedo decreases gradually from 0.3 to 0.2 and the lower albedo in the north compared to the south is most probably due to different concentrations of volcanic dust, with high concentrations in the north and low concentrations in the south. The northern glaciers lie in a volcanically active area and are bordered by an extensive plain of volcanic dust and lava-fields.

Table III. Snow line elevation (SLE) extracted from the AVHRR image of 8 September 1996 for five outlet glaciers. The equilibrium line altitude (ELA) is given for three of the glaciers. The ELA is the mean ELA over 1994 to 1996 (Björnson(1990)).

	SLE (8 Sept. 1996) (m a.s.l.)	ELA (m a.s.l.)
Breidamerkurjökull	950	
Skeidararjökull	1050	
Bruarjökull	1175	1153
Dyngjujökull	1300	1215
Koldukvislarjökull	1325	1303

The snow-line is clearly visible in all images. Using an elevation model of the ice cap, we estimated the snow-line elevation (SLE) during the season, which varies in height for different glaciers of the ice cap. Table III shows the SLE for five glaciers derived from the AVHRR image of 8 September, 1996. Furthermore, the Table gives the mean equilibrium line altitude (ELA) for these glaciers as presented by Björnson(1990). In general, the SLE at the end of the melting season gives an indication of the ELA, provided there is no superimposed ice present on the glacier. According to Williams *et al.*(1991) the superimposed ice zone does not exist on glaciers of the temperate type such as the Vatnajökull. The presented SLE are comparable to the ELA, and therefore we can assume that the SLE on 8 September is approximately the ELA for 1996. The differences in SLE between north and south are probably caused by differences in amount of precipitation (Williams(1987)); in the north the annual mean precipitation is 600 to 1200 mm compared to over 4000 mm in the south.

4.3. COMPARISON OF AVHRR-DERIVED SURFACE ALBEDO AND GROUND-BASED MEASUREMENTS

Figure 5 shows the satellite-derived (both AVHRR and TM) and the in-situ measured (with both pyranometer and portable albedometer) surface albedo at every site as a function of time. To allow for the uncertainty in geolocation of the images we use satellite-derived albedos that are means of nine pixels around the meteorological site; the error bar indicates the spread in these nine pixel values. The ground-based measurements are extracted from the time series at the overpass time of the satellite, with the error bar indicating the measurement error of 3% in the irradiances. The

figure shows that the AVHRR is able to reproduce the development over time fairly well. Nevertheless, large differences in surface albedo occur at some of the sites.

For snow-covered surfaces with no snow-line in the vicinity the differences in surface albedo between AVHRR-derived and ground-based measurements are small, ± 0.05 . This is the case near U7, R5 and for the first half of the melt season near U8. When the snow-line is in the vicinity, the differences and the spread become larger (± 0.15) regardless of the fact that snow does not always cover the surface near the site. Good examples are sites U8 around 20 August and U9 and R2 around 20 June. The differences and large spread are due to the snow-line crossing the 3×3 areas producing a large spread over the set of measurements. When the snow-line is positioned at a lower elevation than the site, the satellite-derived albedo is lower than the ground-based measurements; an example is R2 around 20 June where the site lies approximately 50 m higher than the snow-line. When the snow-line lies higher than the site the satellite-derived albedo is higher than the in-situ measurements; examples are site U8 around 20 August where the site lies approximately 50 m lower than the snow-line and U9 around 20 June where the site also lies approximately 50 m lower than the snow-line. Sites U8, U9, R4 and R5 show a distinct increase in surface albedo around 25 August, almost certainly caused by fresh snow that fell one or two days before the satellite overpass.

When bare ice becomes exposed the albedo differences are variable. For sites A4, A5 and R4 the albedo differences are of the order of 0.15, the in-situ measured albedo being larger than the satellite-derived albedo. For sites I6, U9 and R2 the differences are of the order of 0.06. Knap and Oerlemans(1996) obtained comparable results for the ablation zone of the Greenland ice sheet (their Figure 2b), and suggested that albedo variations on sub-pixel scale are responsible for the large systematic differences found between satellite-derived and in-situ measured albedo. In the case presented here the in-situ measurements of the surface albedo for sites A4, A5 and R4 were made on relatively clean (high albedo) areas compared to the surrounding 1×1 km. This could explain why the albedo appears to be biased to higher values for the in-situ measured albedo compared to the surrounding 1×1 km for these sites. The physical composition of the surface around sites I6, U9 and R2 is more homogeneous, and this could explain why for these sites the albedo is not biased but is in reasonably good agreement with the albedo of the surrounding 1×1 km.

4.4. COMPARISON OF TM-DERIVED SURFACE ALBEDO AND GROUND-BASED MEASUREMENTS

To examine the variability in the surface albedo on smaller scales than the AVHRR pixel size (1×1 km) and to see whether a satellite image with smaller pixel size is able to reproduce the in-situ measured albedo, we made a comparison between TM-derived albedos and ground-based measurements. Unfortunately, cloud cover makes it difficult to find suitable matching images, but for the 1996 melt season one image was found which was good enough for our purpose. Except for sites R4 and

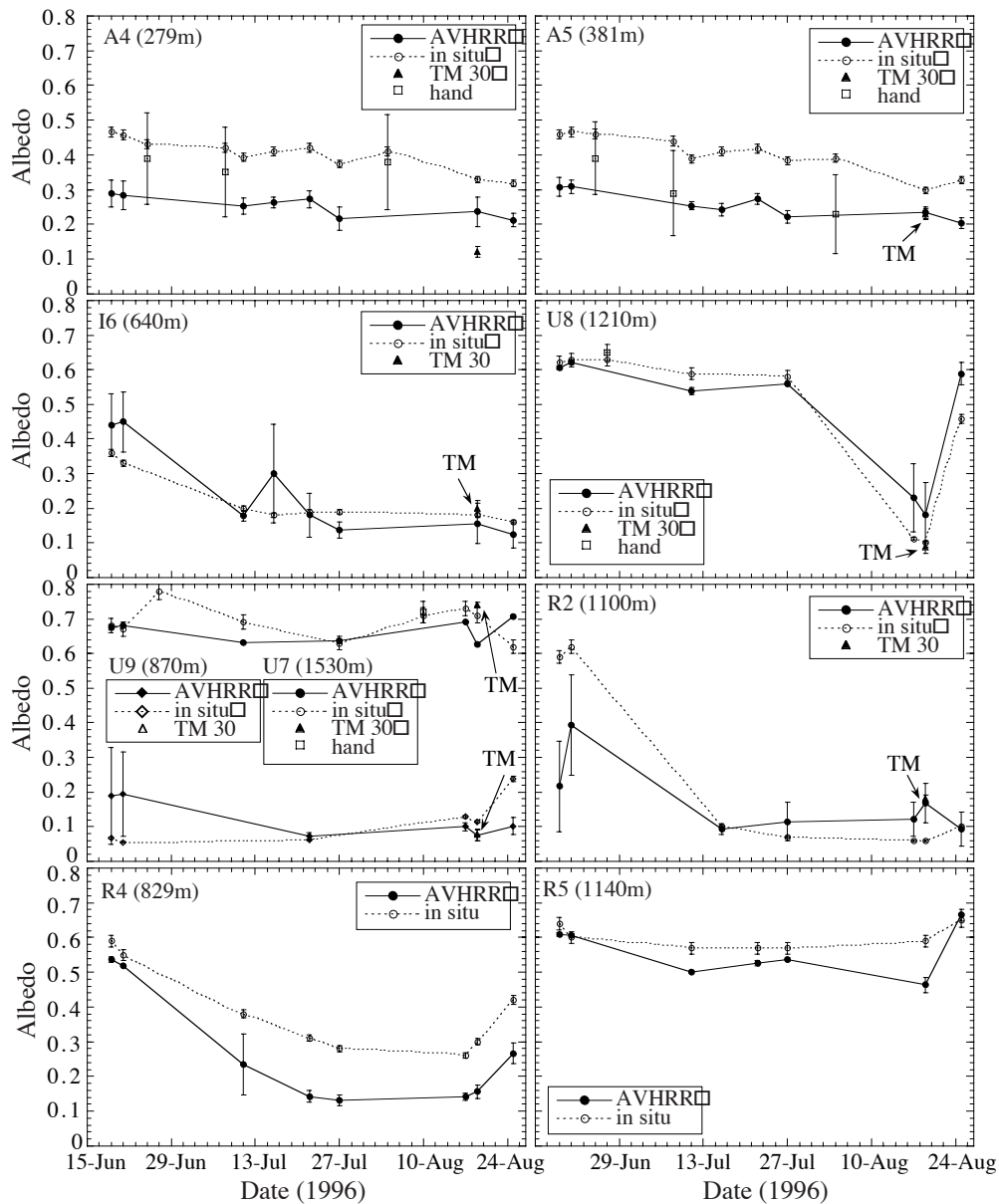


Figure 5. Satellite-derived and in-situ measured surface albedo as a function of time. The satellite-derived albedo is the mean of nine pixels around the meteorological site, the error bar is the spread in these nine points. The in-situ measured albedos are extracted from the time series at AVHRR overpass time and the error bars indicate the measuring error of 3% in the irradiances. When available, portable albedo measurements (sites A4, A5, U7 and U8) and TM measurements (sites A4, A5, I6, U7, U8, U9 and R2) are included. Site U7 and U9 are plotted in the same figure.

R5 it was possible to derive a TM albedo value for each site from this image, and the values are plotted in Figure 5 as averages of nine pixels around the meteorological site. The error bar indicates the spread in these nine pixel values.

For sites I6 and U9 the TM-derived albedo is in reasonably good agreement with the ground-based measurements as well as the AVHRR-derived albedo (within a range of 0.05). The TM-derived albedo and the in-situ measurements near site U8 are also in reasonably good agreement, noting that the snow-line does not cross the 3×3 TM area. At these three sites the variability in surface albedo is low (as mentioned earlier), whilst for sites A4, A5 and R2 the difference between TM-derived and ground-based measurements is larger (> 0.10). It seems that the in-situ measurements of the surface albedo for these sites were not only made on relatively clean, high albedo, areas compared to the surrounding 1×1 km, but compared to the surrounding 30×30 m the measured surface was also relatively clean. To obtain a better insight into the variability of the TM-derived albedos, and to see whether the uncertainty in the geolocation can produce the differences, we show in Figure 6 the distributions of 9×9 albedo values surrounding the sites. This figure shows that in three cases (I6, U8 and U9) the in-situ value is represented by a TM value. For sites A4, A5 and R2 the outer limits of the distributions do not coincide with the in-situ measured albedo. Therefore, geolocation problems cannot cause the large systematic difference, and albedo variations for these sites occur probably on scales smaller than the TM pixel size. Up to now the analysis has been made on the assumption that the retrieval method gives accurate values of the surface albedo, which is not necessarily true. Especially the isotropic assumption may have contributed significantly to the observed differences, particularly because the assumption has a large impact on the ice albedo compared to the snow albedo. The uncertainties in the retrieval method probably explain only part of the differences found.

To obtain a better idea of the sub-pixel scale variations we measured the surface albedo around four sites (A4, A5, U7 and U8) using a portable albedometer (Figure 2). The surface around sites U7 and U8 was snow-covered during the measurements, while the surface around A4 and A5 consisted of bare ice. Figure 5 also shows the portable albedo measurements, together with the ground and satellite measurements. The portable albedo measurements given are the mean of 25 points measured on a grid of 40×40 m around the pyranometer, noting that the error bar is the spread in these 25 points. For the snow-covered surfaces the spread is small, as expected (± 0.05); the spread in the measurements of ± 0.12 for the ice surface near A4 and A5 is larger. The portable albedo measurements indicate a large variability on a scale of several metres. A site could have been chosen such that ground-based measurements were much closer to AVHRR or TM. So the large systematic difference between satellite and in-situ derived surface albedo may be due to albedo variations on scales comparable to, or larger than, the size of the surface viewed by the pyranometer and smaller than the pixel size of the satellite. This confirms the hypothesis of Knap and Oerlemans(1996).

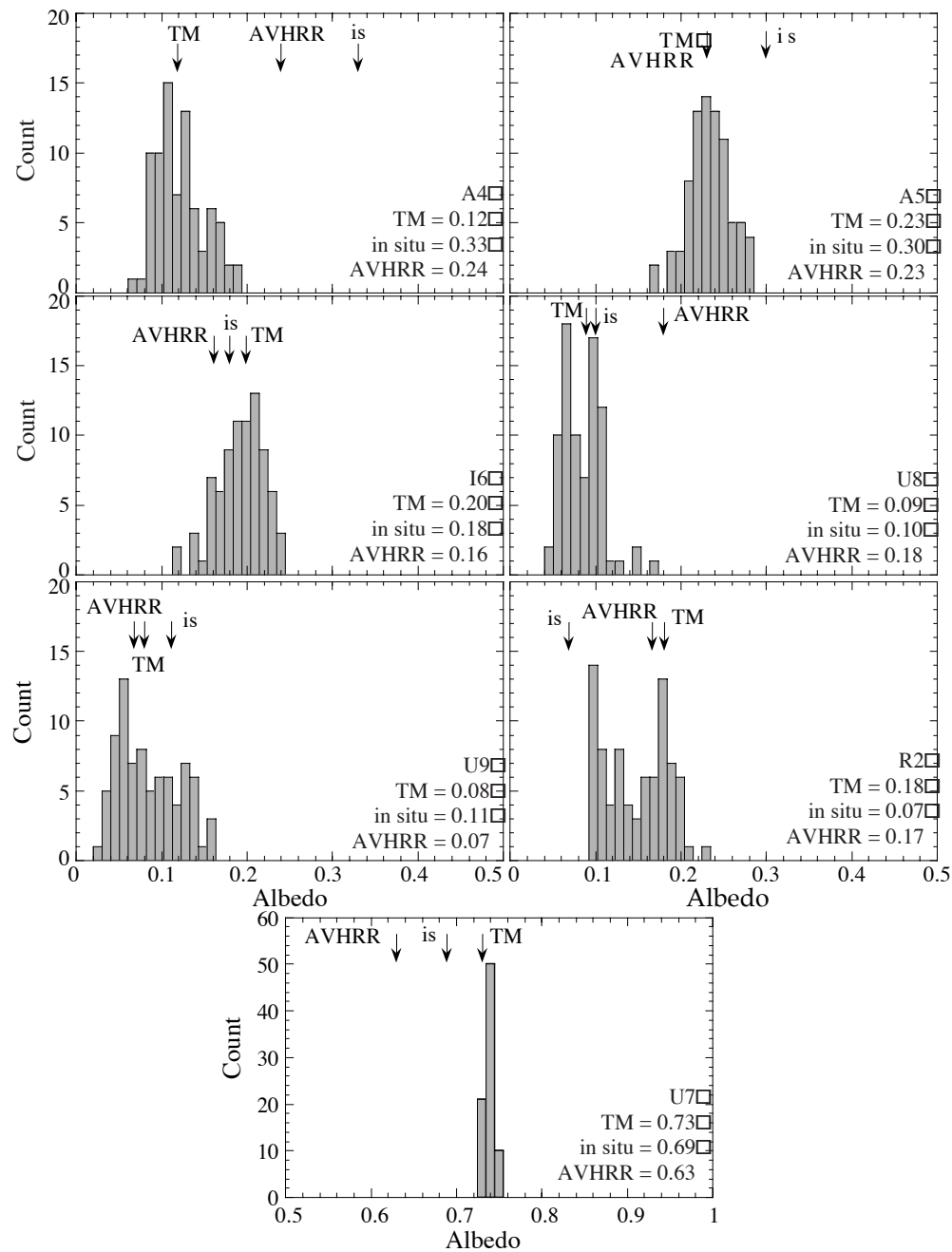


Figure 6. TM-derived albedo distribution of 9×9 pixels around the possible site position on 19 August 1996. The TM values of the centre pixel is presented as well as the AVHRR-derived albedo and the in situ albedo (is) extracted from the time series at TM overpass time.

Table IV. Some relevant parameters of the TM and AVHRR images used in the comparison. θ_s is the solar zenith angle at overhead time.

Date	Instrument	Overhead time (UTC)	θ_s°
17-7-1995	TM	1130	53.8
	AVHRR	1340	50.9
19-8-1996	TM	1143	53.9
	AVHRR	1412	53.4

4.5. COMPARISON OF AVHRR-DERIVED AND TM-DERIVED SURFACE ALBEDO

To examine the influence of pixel size in more detail, we compared the AVHRR-derived surface albedos with TM-derived surface albedos (1×1 km versus 30×30 m pixel size). The pixel size of the TM is closer to the size of the surface area viewed by the pyranometer than the AVHRR pixel size. For the comparison two TM images with matching AVHRR images are selected (Table IV). To compare AVHRR-derived and TM-derived surface albedo a south-north transect (transect no. 1, Figure 1) parallel to the south-north transect of the field experiment of 1996 is extracted from the images (Figure 7). The transect has a length of about 100 km and contains the Breidamerkurjökull in the south and the Dyngjujökull in the north. The values are averages of 3 pixels perpendicular to the transect and a 3-point running mean along the transect. The TM (1 km) transect is extracted from the TM image averaged to pixels of 1×1 km.

Figure 7 shows that, in general, the TM-derived albedo for snow surfaces (between 20 and 80 km distance from the southern margin) is larger than the AVHRR-derived albedo. For ice surfaces (between 0 and 20 km, and 80 and 100 km from the southern margin) they are of the same order of magnitude. Although the variability of the albedo in the TM transect is larger for ice surfaces than for snow surfaces the TM images cannot explain the large difference in albedo found between the in-situ measurements and the satellite-derived measurements found for sites A4, A5 and R4. The overall pattern of the transects is similar. Due to geolocation problems the positioning of the two transects is not exactly the same as evidenced in the transition from lower to higher albedos around 15 and 80 km from the ice edge. Another problem in comparing these images is the timing - the AVHRR image is acquired 2 to 2.5 hours after the TM image, so the solar zenith angles are different. On the TM image of 19 August 1996 in channel 7 (2.08 - 2.35 μ m) a haze is visible on the top of the ice cap. In the AVHRR image of 2.5 hours later the haze has disappeared. Such a haze can explain the larger difference between TM and AVHRR data in August 1996 compared to August 1995. Furthermore, the AVHRR images reveal no clouds

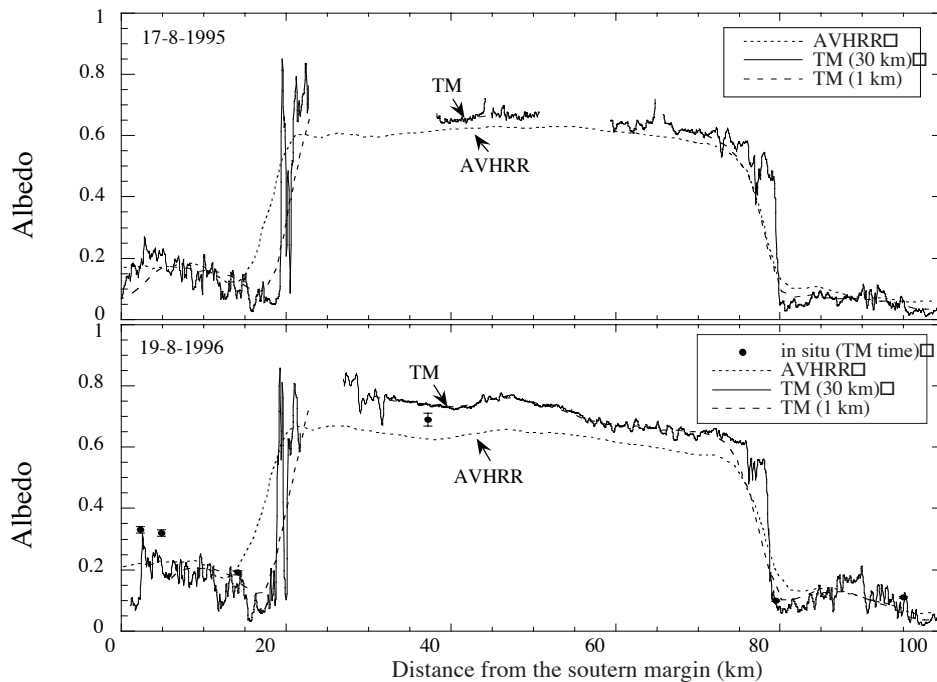


Figure 7. AVHRR-derived and TM-derived surface albedo over a south-north transect of the ice cap. The albedo is given as a function from the distance to the southern ice-margin. Parts of the transect are missing due to possible cloud cover. When available, ground measurements are included.

or haze, whereas the TM transects show gaps that represent possible cloud cover. It is unlikely that other passes are similarly affected by haze because the haze would be visible in the mid-infrared or thermal-infrared channels of the satellite instruments.

5. Summary and concluding remarks

An analysis of the temporal and spatial variations in the surface albedo of the Vatnajökull ice cap, Iceland, derived from satellite-based (AVHRR and TM) and ground-based measurements is presented here. It shows that satellite data can indeed provide a representative two-dimensional image of the surface albedo of the ice cap. The spatial variations are better described this way than using only a few point measurements. The analysis also shows that, in general, the satellite instruments are able to reproduce the variations in time fairly well although large systematic differences between these measurements and the ground-based measurements occur for some of the sites on ice.

These differences are attributed to sub-pixel-scale variations in the surface albedo. The scale of coverage of the ground measurements is small compared to the pixel size of the TM or AVHRR (about 10 m compared to 30 m and 1 km, respectively).

The snow albedo is generally not highly variable; the ice albedo on the other hand can have a high spatial variability over distances of only a few metres, causing the ground measurements and satellite measurements to differ considerably. It is shown that the TM pixel size is still too large to represent the ground measurements accurately. In the case presented here, the in-situ measurements of the surface albedo seem to be biased because the measurements were made on relatively clean, high albedo, areas compared to the surrounding 30×30 m.

It is worth to note that the analysis presented here is hampered by the fact the overpass time of the NOAA and Landsat satellites differ, and cloud cover conditions can change significantly in a few hours. Furthermore, the difference between satellite-derived surface albedo and in-situ measured surface albedo was discussed on the assumption that the retrieval method presented in Section 3 gives accurate values of the surface albedo. This is not necessarily true, of course. The atmosphere correction, the assumption of an isotropic reflected radiation field and the spectral integration are all potential sources of errors. Knap and Oerlemans(1996), Knap *et al.*(1998) and Knap and Reijmer(1998) discuss some errors related to the retrieval of the surface albedo from satellite measurements. The latter authors suggest that significant errors in satellite-derived albedos may arise from the assumption that the reflected radiation field is isotropic. The impact of this assumption is larger for ice albedos than for snow albedos. In conclusion we may therefore state that, apart from sub-pixel variation, uncertainties in the retrieval method, especially the isotropic assumption, may have contributed to the observed differences between satellite-derived and ground-based measurements.

Acknowledgements

Financial support for this project was provided by the European Union project TEMBA (Climate sensitivity of glacier mass balance: the effect of topographic barriers) contract ENV4-CT95-0105. The investigations were also (in part) supported by the Netherlands Geosciences Foundation (GOA) with financial aid from the Netherlands Organisation for Scientific Research (NWO).

References

- Ambach, W., 1963. Untersuchungen zum energieumsatz in der ablationszone des GrnLndischen inlandeises (camp IV-EGIG, 69°4005N, 49°3458W). *Medd. GrønL.*, **174**(4).
- Björnson, H., 1990. Mass balance of polar regions. *IASC Report*, **5**, 25–29.
- Epema, G. F., 1990. Determination of planetary reflectance for Landsat-5 Thematic-Mapper tapes processed by Earthnet (Italy). *ESA Journal 1990*, **14**, 101–107.
- Hall, D. K., R. A. Bindshadler, J. L. Foster, A. T. C. Chang and H. Siddalingaiah, 1990. Comparison of in situ and TM-derived reflectance of Forbindels Glacier, Greenland. *Int. J. Remote Sens.*, **11**(3), 493–504.

- Houghton, J. T., L. G. M. Filho, B. A. Callander, N. Harris, A. Kattenberg and K. Maskell, editors, 1995. *Climate Change 1995: The Science of Climate Change. Contribution of Working Group I to the Second Assessment Report of the Intergovernmental Panel on Climate Change*. Cambridge University Press, Cambridge, UK.
- Knap, W. H. and J. Oerlemans, 1996. The surface albedo of the Greenland ice sheet: Satellite-derived and in situ measurements in the Søndre Strømfjord area during the 1991 melt season. *J. Glaciol.*, **42**(141), 364–374.
- Knap, W. H. and C. H. Reijmer, 1998. Anisotropy of the reflected radiation field over melting glacier ice: Measurements in Landsat TM bands 2 and 4. *Remote Sens. Environ.*, **65**, 93–104.
- Knap, W. H., B. W. Brock, J. Oerlemans and I. C. Willis, 1998. Comparison of Landsat-TM derived and ground-based albedos of Haut Glacier d’Arolla, Switzerland. *Int. J. Remote Sens.*, **20**(17), 3293–3310.
- Knap, W. H., C. H. Reijmer and J. Oerlemans, 1999. Narrowband to broadband conversion of Landsat-TM glacier albedos. *Int. J. Remote Sens.*, **20**(10), 2091–2110.
- Koelemeijer, R., J. Oerlemans and S. Tjemkes, 1993. Surface reflectance of Hintereisferner, Austria, from Landsat 5 TM imagery. *Ann. Glaciol.*, **17**, 17–22.
- Li, Z. and H. G. Leighton, 1992. Narrowband to broadband conversion with spatially autocorrelated reflectance measurements. *J. Appl. Meteorol.*, **31**, 421–432.
- Lillesand, T. M. and R. W. Kiefer, 1987. *Remote Sensing and Image Interpretation*. John Wiley and Sons, Inc., second edition. 721 pp.
- McClatchey, R. A., R. W. Fenn, J. E. A. Selby and J. S. Garing, 1972. Optical properties of the atmosphere. *Environ. Res. Papers*, **411**. AFCRL-72-0497.
- Reijmer, C. H., 1997. *The Surface Albedo of the Vatnajökull Ice Cap, Iceland: a Comparison Between Satellite-Derived and In Situ Measurements*. Master’s thesis, IMAU, Utrecht University. Internal Report, V97-11.
- Slingo, A. and H. M. Schrecker, 1982. On the shortwave radiation properties of stratiform water clouds. *Quart. J. Roy. Meteorol. Soc.*, **108**, 407–426.
- Suttles, J. T., R. N. Green, P. Minnis, G. L. Smith, W. F. Stayler, B. A. Wielicki, I. J. Walker, D. F. Young, V. R. Taylor and L. L. Stone, 1988. Angular radiation models for Earth-atmosphere system. volume 1: Shortwave radiation. In: *NASA reference Publication 1184*. NASA, Washington, DC.
- TEMBA, 1997. *First Annual Report to the European Commission on the Project: Climate Sensitivity of Glacier Mass Balance: the Effect of Topographic Barriers*. 61 pp.
- Thome, K. J., D. I. Gellman, R. J. Parada, S. F. Biggar, P. N. Slater and M. S. Moran, 1993. In-flight radiometric calibration of Landsat-5 Thematic Mapper from 1984 to present. In: *Soc. of Photo-Optical Instrum. Eng. Symp.*, pages 126–130. 12-16 April, Orlando, FL.
- Van der Hage, J. C. H., 1992. Interpretation of field measurements made with a portable albedometer. *J. Atmos. Oceanic Tech.*, **9**, 420–425.
- Williams, R. S., 1987. Satellite remote sensing of the Vatnajökull, Iceland. *Ann. Glaciol.*, **9**, 127–135.
- Williams, R. S., D. K. Hall and C. S. Benson, 1991. Analysis of glacier facies using satellite techniques. *J. Glaciol.*, **37**(125), 120–128.